JOURNAL OF INFORMATION PROCESSING SYSTEMS JIPS

Fuzzy Neural Network Active Disturbance Rejection Control for Two-Wheeled Self-Balanced Robot

Chao Wang, Xiao Jianliang*, and Cheng Zhang

Abstract

Considering the problems of poor control effect, weak disturbance rejection ability and adaptive ability of two-wheeled self-balanced robot (TWSBR) systems on undulating roads, this paper proposes a fuzzy neural network active disturbance rejection controller (FNNADRC), that is based on fuzzy neural network (FNN) for online correction of active disturbance rejection controller (ADRC)'s nonlinear control rate. Firstly, the dynamic model of the TWSBR is established and decoupled, the extended state observer (ESO) is used to compensate dynamically and linearize the upright and displacement subsystems. Then, the nonlinear PD control rate and FNN are designed, and the FNN is used to modify the control parameters of the nonlinear PD control rate in real time. Finally, the proposed control strategy is simulated and compared with the traditional ADRC and fuzzy active disturbance rejection controller (FADRC). The simulation results show that the control effect of the proposed control strategy is slightly better than ADRC and FADRC.

Keywords

ADRC, Compensate Dynamically, ESO, FNN, Nonlinear PD Control Rate, TWSBR

1. Introduction

Two-wheeled self-balanced robots (TWSBRs) are characterized by simple structure, small size, light weight and flexible movement, so it has been widely applied in different industry fields, such as duty patrol, industrial transportation, daily travel [1]. As a multi-purpose load-bearing tool, TWSBR needs to adapt to different terrains. Dynamic disturbing forces will be generated at contact points between wheels and different ground. These disturbances are caused by the change of the contact angle between the wheel and the ground. Currently, many control methods have been proposed for TWSBRs [2-8]. In these references, proportional-integral-derivative (PID), linear quadratic regulator (LQR), neural network and other control methods are used, but they are all based on the mathematical model which is on the plane. Because most strategies have unsatisfactory disturbance rejection and adaptive ability, it is difficult to apply a TWSBR to slope road surfaces, undulating road surfaces and other complex working environments. Therefore, how to enhance the control ability of the control strategy is the problem that needs to be solved.

In 2014, Hu and Yan [9] estimated the perturbation of the dynamic system through a system state observer and designed the controller combined with LQR approach, which improved the disturbance

rejection effect to a certain extent. In 2016, Jiang et al. [10] proposed an adaptive differential active disturbance rejection controller (ADRC), which adjusted the parameters of ADRC through an adaptive differential evolution algorithm, however, only the compensation factor is adjusted without considering the adjustment of control rate parameters and observer parameters [10]. In 2017, Unluturk and Aydogdu [11] proposed an adaptive switch controller based on the neural network, which realized the balance control under the soil pavement, pebble pavement, and sand and gravel pavement, without considering the slope and undulating pavement. In the same year, Liang et al. [12] established the dynamic TWSBR model on the undulating pavement surface, and designed a LQR controller. The convergence speed of the controller needs to be improved [12]. In 2020, Tran et al. [13] proposed a simple controller based on a composite observer for trajectory tracking and balance control with unknown disturbance of input and uncertain functions of a TWSBR model. Then, the closed-loop control system's stability is proved, and a simulation comparison is made at last. In the same year, Karam et al. [14] designed a robust controller and used state feedback to estimate the equivalent term of SMC control law to overcome the dependence of the model. The simulation results show that the property of SFSMC is better than that of classical SMC in terms of tracking error. In 2021, Fikri et al. [15] designed the H_∞ controller. The research shows that the H_∞ controller has satisfactory disturbance rejection performance. None of the above research methods considers how to enhance the anti-interference capability and adaptive ability of the TWSBR on undulating road surface. Therefore, this paper proposes a control strategy for the TWSBR on undulating road surface.

We present a fuzzy neural network active disturbance rejection controller (FNNADRC) strategy for a TWSBR under complex road conditions in this paper. In order to improve the disturbance rejection capability of the TWSBR, the disturbance is estimated and compensated by the extended state observer (ESO) in ADRC method. The parameters of nonlinear PD control rate are fixed, which leads to its weak adaptive ability. Combining neural network and fuzzy control makes the network have both self-learning ability and reasoning ability [16], so as to correct the control parameters of nonlinear PD control rate in real time according to the size of control error and error rate of change. In this way, the control effect is improved, so that it can move stably in complex road conditions.

The advantages of this study can be summarized as follows:

On the basis of traditional ADRC control, the idea of fuzzy neural network (FNN) is integrated. According to the state error, the ADRC parameters are adjusted in real time to overcome the serious interference of TWSBR control systems under complex road conditions. By using the self-learning advantage of FNN, the problem that parameters need to be adjusted through certain exploration experience in fuzzy control is solved.

This paper is organized as follows: Section 2 discusses the TWSBR model under rolling pavement. In Section 3, we propose the FNNADRC based ESO. In Section 4, the superiority of FNNADRC method is compared by simulation. Section 5 concludes this.
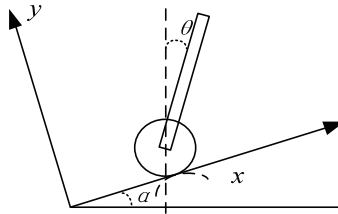
2. Dynamic Model

Fig. 1 shows the TWSBR on the undulating pavement. The special case of the undulating road is the slope road; therefore, the undulating road can be regarded as the slope road whose inclination angle

changes continuously and slowly [12]. The schematic diagram of instantaneous movement of the TWSBR on undulating road surface is shown in Fig. 2.
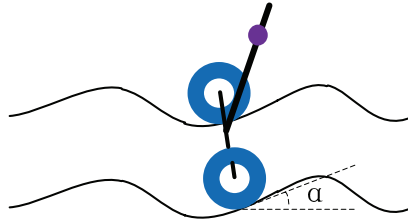
Fig. 1. TWSBR on the undulating road.

Fig. 2. Forward motion schematic diagram.

In this case, the dynamic model can be expressed as follows:

$$\begin{cases} \dot{x}_1 = x_2 \\ \dot{x}_2 = \dfrac{B_1 + B_2 - B_3 - B_4}{A} \\ \dot{x}_3 = x_4 \\ \dot{x}_4 = \dfrac{(u_1 - u_2)dr}{a_3} \\ \dot{x}_5 = x_6 \\ \dot{x}_6 = \dfrac{C_1 - C_2 - C_3 - C_4 + C_5}{A} \end{cases} \tag{1}$$

where,

$$B_1 = a_1[M_B gl\sin(x_1 + \theta_\varepsilon) + M_B x_6 l\sin(x_1 + \alpha + \theta_\varepsilon)\dot{\alpha}]$$
$$B_2 = a_4(2M_W + M_B)rg\sin\alpha \cos(x_1 + \alpha + \theta_\varepsilon)$$
$$B_3 = a_4{}^2 x_2(x_2 + \dot{\alpha}) \sin(x_1 + \alpha + \theta_\varepsilon) \cos(x_1 + \alpha + \theta_\varepsilon)$$
$$B_4 = [a_1 + a_4 \cos(x_1 + \alpha + \theta_\varepsilon)](u_1 + u_2)$$
$$A = a_1 a_2 - a_4{}^2 \cos^2(x_1 + \theta_\varepsilon + \alpha)$$
$$C_1 = a_2 a_4 rx_2 \sin(x_1 + \theta_\varepsilon + \alpha)(x_2 + \dot{\alpha})$$
$$C_2 = a_2(M_B + 2M_W)gr^2\sin\alpha$$
$$C_3 = a_4{}^2 g \sin(x_1 + \theta_\varepsilon) \cos(x_1 + \alpha + \theta_\varepsilon)$$
$$C_4 = a_4{}^2 x_6 \dot{\alpha} \sin(x_1 + \alpha + \theta_\varepsilon) \cos(x_1 + \alpha + \theta_\varepsilon)$$
$$C_5 = [a_2 r + a_4 r \cos(x_1 + \alpha + \theta_\varepsilon)](u_1 + u_2)$$
$$a_1 = M_B r^2 + 2M_W r^2 + 2I$$
$$a_2 = M_B l^2 + J$$
$$a_3 = M_W d^2 r^2 + Id^2 + 2Kr^2$$
$$a_4 = M_B lr$$
$$\theta_\varepsilon = \arcsin\frac{(2M_W + M_B)r\sin\alpha}{M_B l}$$
$$x_1 = \theta - \theta_\varepsilon, x_2 = \dot{\theta}, x_3 = \varphi, x_4 = \dot{\varphi}, x_5 = x, x_6 = \dot{x}, u_1 = T_L, u_2 = T_R,$$

θ is pitch angle, φ is yaw angle, x is displacement, T_L is left wheel's torque, T_R is right wheel's torque, α is the angle between the tangent line of the wheel and the road surface and the horizontal line. Table 1 shows the values of relevant parameters.

Table 1. Model parameters

Parameter	Description	Value
M_W	Mass of wheel	0.05 kg
M_B	Mass of body	1.125 kg
I	Torque of the wheel	4.77×10^{-5} kg·m²
J	Inertia of the body rotating about the motor axis	5.19×10^{-3} kg·m²
K	Inertia of the body rotating about the pendulum	6.3×10^{-3} kg·m²
r	wheel radius	0.035 m
l	Center distance of the robot body and the motor axis	0.053 m
d	Wheel axle distance	0.24 m

3. Controller Design

3.1 System Structure Design

The overall structure of FNN control system is shown in Fig. 3.
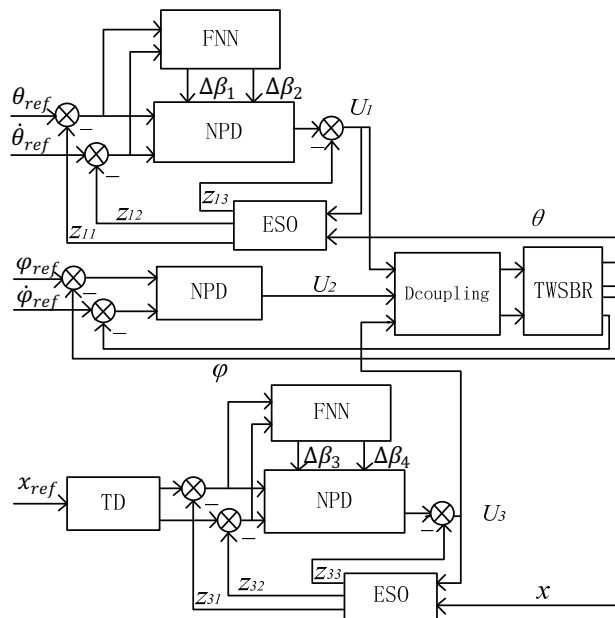
Fig. 3. Fuzzy neural network control block diagram of two-wheeled self-balanced robot.

The TWSBR control system has three subsystems: upright control, turning control and displacement control. The three subsystems are connected through the "static coupling" matrix. According to the separation principle of ADRC design, ADRCs are proposed for the upright and displacement subsystem respectively. In addition, the transition process is implemented by a tracking differentiator (TD), the ESO

and error feedback control law are designed. Since the disturbance model is not included in the turning subsystem, a simple PD control approach is presented for the system. Based on the traditional ADRC of upright subsystem and displacement subsystem, two FNNs with the same structure are introduced respectively. The error of angle and angle error rate of change, the error of displacement and displacement error rate of change are taken as the inputs of the two networks, and the outputs of the two networks are used to regulate the parameters of the nonlinear PD control rate, so as to enhance the disturbance rejection ability of the system.

3.2 MIMO System Decoupling

From the above expression, it can be concluded that the system is a multiple-input and multiple-out (MIMO) coupled system. In order to use decoupling control for a multivariable system, the system is expressed in the following form:

$$\begin{cases} \dot{x}_1 = x_2 \\ \dot{x}_2 = f_1(x_1, x_2, x_6, \alpha) + b_{11}(x_1, \alpha)u_1 + b_{12}(x_1, \alpha)u_2 \\ \dot{x}_3 = x_4 \\ \dot{x}_4 = f_2 + b_{21}u_1 - b_{22}u_2 \\ \dot{x}_5 = x_6 \\ \dot{x}_6 = f_3(x_1, x_2, x_6, \alpha) + b_{31}(x_1, \alpha)u_1 + b_{32}(x_1, \alpha)u_2 \end{cases} \tag{2}$$

where,

$$f_1(x_1, x_2, x_6, \alpha) = \frac{B_1 + B_2 - B_3}{A}$$
$$f_2 = 0$$
$$f_3(x_1, x_2, x_6, \alpha) = \frac{C_1 - C_2 - C_3 - C_4}{A}$$
$$b_{11}(x_1, \alpha) = b_{12}(x_1, \alpha) = \frac{-[a_1 + a_4 \cos(x_1 + \alpha + \theta_\varepsilon)]}{a_1 a_2 - a_4{}^2 \cos^2(x_1 + \theta_\varepsilon + \alpha)}$$
$$b_{21} = -b_{22} = \frac{dr}{a_3}$$
$$b_{31}(x_1, \alpha) = b_{32}(x_1, \alpha) = \frac{[a_2 r + a_4 r \cos(x_1 + \alpha + \theta_\varepsilon)]}{a_1 a_2 - a_4{}^2 \cos^2(x_1 + \theta_\varepsilon + \alpha)}.$$

According to expression (2), the amplification coefficient matrix of the control force is

$$B = \begin{bmatrix} b_{11}(x_1, \alpha) & b_{12}(x_1, \alpha) \\ b_{21} & b_{22} \\ b_{31}(x_1, \alpha) & b_{32}(x_1, \alpha) \end{bmatrix} \tag{3}$$

Virtual control variables U_1, U_2, U_3 are introduced, and the input-output relationship of each channel is

$$\begin{cases} \dot{x}_1 = x_2 \\ \dot{x}_2 = f_1(x_1, x_2, x_6, \alpha) + U_1 \\ \dot{x}_3 = x_4 \\ \dot{x}_4 = f_2 + U_2 \\ \dot{x}_5 = x_6 \\ \dot{x}_6 = f_3(x_1, x_2, x_6, \alpha) + U_3 \\ y_1 = x_1, y_2 = x_3, y_3 = x_5 \end{cases} \tag{4}$$

In this way, the relationship between the virtual control signal of each channel and the controlled output is single-input and single-output (SISO). Each channel's output and the intermediate control signal are perfectly decoupled, and the controller of each subsystem should be presented on the basis of the approach of the SISO system.

The real control signal can be expressed as follows:

$$u = X_B U \tag{5}$$

Select the x_1 in sight of the equilibrium point, $x_1 = 0$, $\alpha = 0$ can be selected to calculate the approximate value of B. Then calculate the inverse of B, since B is irreversible in this system, the pseudo-inverse matrix X_B is calculated for B.

3.3 Design of ADRC

3.3.1 Design of ADRC for the upright subsystem

After the system is decoupled, the expression of the upright subsystem is

$$\begin{cases} \dot{x}_1 = x_2 \\ \dot{x}_2 = f_1(x_1, x_2, x_6, \alpha) + U_1 \end{cases} \tag{6}$$

The expected angle value of the subsystem is 0, so it is not necessary to have the tracking differentiator. Only the nonlinear control rate and ESO need to be designed, and then the dynamic compensation linearization is carried out. The ESO of the upright subsystem is

$$\begin{cases} e = z_{11} - y_1 \\ \dot{z}_{11} = z_{12} - \beta_{11}e \\ \dot{z}_{12} = z_{13} - \beta_{12}fal(e, 0.5, \delta) + U_1 \\ \dot{z}_{13} = -\beta_{13}fal(e, 0.25, \delta) \end{cases} \tag{7}$$

where,

$$fal(e, \gamma, \delta) = \begin{cases} |e|^\gamma sign(e), |e| > \delta \\ {e}/{\delta^{\gamma-1}}, |e| \leq \delta \end{cases}$$

z_{11} is the estimation of the system output, z_{12} is the estimation of system state x_1, z_{13} is the estimation of system state x_2.

The nonlinear PD control rate of the upright subsystem is

$$u_{10} = \beta_1 fal(e_1, \alpha_1, \delta) + \beta_2 fal(e_2, \alpha_2, \delta) \\ 0 < \alpha_1 < 1 < \alpha_2 \tag{8}$$

where, β_1, β_2 are the parameters of nonlinear PD control rate.

Because it is necessary to design the FNN to correct β_1, β_2 in real time according to the inclination error signal and inclination velocity error signal, the correction parameters $\Delta\beta_1, \Delta\beta_2$ are introduced. The values are directly applied to the original control rate parameter to modify it. Therefore, the expression (8) is written as follows:

$$u_{10} = (\beta_1 + \Delta\beta_1)fal(e_1, \alpha_1, \delta) + (\beta_2 + \Delta\beta_2)fal(e_2, \alpha_2, \delta) \tag{9}$$

The compensation of the disturbance for the upright subsystem is

$$U_1 = u_{10} - z_{13}. \tag{10}$$

3.3.2 Design of PD for the turning subsystem

When the dynamic system is decoupled, the expression of the turning subsystem is

$$\begin{cases} \dot{x}_3 = x_4 \\ \dot{x}_4 = f_2 + U_2 \end{cases} \tag{11}$$

Since the turning subsystem is a plain integrator series system, the control system of upright and displacement has little negative effect on the turning subsystem, the simple PD approach is adopted for the turning subsystem.

$$U_2 = K_p(\varphi_r - \varphi) + K_d(\dot{\varphi}_r - \dot{\varphi}) \tag{12}$$

where φ_r is the desirable turning angle and φ is the real turning angle.

3.3.3 Design of ADRC for displacement subsystem

Since the system is decoupled, the displacement subsystem can be expressed as

$$\begin{cases} \dot{x}_5 = x_6 \\ \dot{x}_6 = f_3(x_1, x_2, x_6, \alpha) + U_3 \end{cases} \tag{13}$$

The subsystem of displacement and the subsystem of upright interact with each other. In order to avoid overshoot of the subsystem of displacement and the effect of the upright control, the transition process is arranged. The other designs are similar to the upright subsystem. The TD used to realize the transition process is

$$\begin{cases} \dot{v}_1 = v_2 \\ \dot{v}_2 = -rsign(v_1 - y_3 + \dfrac{v_2|v_2|}{2r}) \end{cases} \tag{14}$$

where, the solution v_1 of the equation can approach y_3 in any finite time, v_2 is the differential signal of v_1.

The ESO of the displacement subsystem is

$$\begin{cases} e = z_{31} - y_3 \\ \dot{z}_{31} = z_{32} - \beta_{31}e \\ \dot{z}_{32} = z_{33} - \beta_{32}fal(e, 0.5, \delta) + U_3 \\ \dot{z}_{33} = -\beta_{33}fal(e, 0.25, \delta) \end{cases} \tag{15}$$

where,

$$fal(e, \gamma, \delta) = \begin{cases} |e|^\gamma sign(e), |e| > \delta \\ {e}/{\delta^{\gamma-1}}, |e| \leq \delta \end{cases}$$

z_{31} is the estimation of the system output, z_{32} is the estimation of system state x_5, z_{33} is the estimation of system state x_6.

The nonlinear PD control rate of the displacement subsystem is

$$u_{30} = (\beta_3 + \Delta\beta_3)fal(e_3, \alpha_3, \delta) + (\beta_4 + \Delta\beta_4)fal(e_4, \alpha_4, \delta) \tag{16}$$

where, β_3 and β_4 are the parameters of nonlinear PD control rate, $\Delta\beta_3$ and $\Delta\beta_4$ are the correction parameters.

The disturbance compensation of displacement subsystem is

$$U_3 = u_{30} - z_{33}. \tag{17}$$

3.4 Design of Fuzzy Neural Network

3.4.1 Structure of fuzzy neural network

The structure of FNN is shown in Fig. 4. The entire network has two inputs and two outputs, there are five layers in total. For the upright and displacement subsystem, the network is applied to adjust the parameters of the control rate respectively.
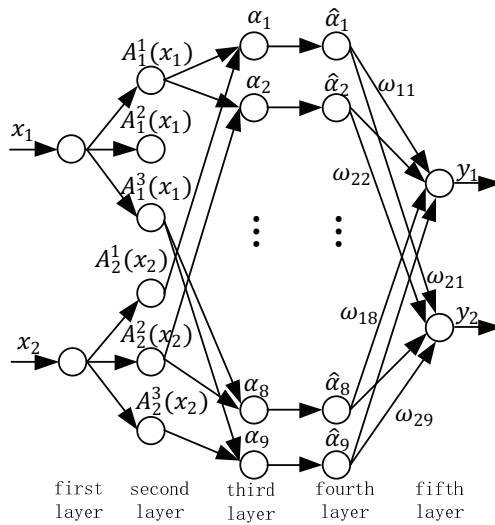
Fig. 4. Fuzzy neural network structure diagram.

The first layer is the input layer which has two nodes. The inputs of the layer are the error and the error rate of the change. Its function is to pass the input to the next layer node.

The second layer is the membership layer which has six nodes, and each input corresponding to the first layer has three fuzzy sets {"negative", "zero", "positive"}. Gaussian functions are adopted as membership functions, then

$$A_i^j(x_i) = \exp\left(-\frac{(x_i - a_{ij})^2}{b_{ij}^2}\right) \tag{18}$$

where $i = 1, 2$; $j = 1, 2, 3$; $A_i^j(x_i)$ indicates that the i-th input corresponds to the j-th linguistic variable value.

The third layer is the inference layer, which has nine nodes, each node represents a fuzzy rule, and the applicability of each rule is calculated as

$$\alpha_l = A_1^{j_1}(x_1) \cdot A_2^{j_2}(x_2) \tag{19}$$

where, j_1=1, 2, 3; j_2=1, 2, 3; l =1, 2, …, 9.

The fourth layer is the normalized layer, which also has nine nodes, and the normalized calculation result is

$$\hat{\alpha}_l = \frac{\alpha_l}{\sum_{i=1}^{9} \alpha_i} \tag{20}$$

where l = 1, 2, …, 9.

The fifth layer is the output layer, which has two nodes for de-fuzzification calculation. The outputs of the layer are correction offsets of control parameters.

$$y_k = \sum_{l=1}^{9} \omega_{kl} \hat{\alpha}_l \tag{21}$$

where, k = 1, 2; ω_{kl} is the weight of the network, y_k is the output of the network, $\Delta\beta_1$=y_1, $\Delta\beta_2$=y_2.

3.4.2 Learning algorithm

The fuzzy segmentation number in this design has been determined, and the parameters to be trained include the connection weight ω_{kl} of the fifth layer, and the center value parameters a_{ij} and b_{ij} of the second layer.

Let the desired output of the system be $\hat{y}_k$, the training objective functions are

$$J = \frac{1}{2}\sum_{k=1}^{2}(\hat{y}_k - y_k)^2. \tag{22}$$

The iterative formulas for adjusting parameters are

$$\omega_{kl}(t + 1) = \omega_{kl}(t) - \eta_1 \frac{\partial J}{\partial \omega_{kl}} \tag{23}$$

where, k = 1, 2; l = 1, 2, …, 9.

$$a_{ij}(t + 1) = a_{ij}(t) - \eta_2 \frac{\partial J}{\partial a_{ij}} \tag{24}$$

where, i = 1, 2, 3; j=1, 2, 3.

$$b_{ij}(t + 1) = b_{ij}(t) - \eta_3 \frac{\partial J}{\partial b_{ij}} \tag{25}$$

where, η_1, η_2, η_3 are the learning rates.

4. Simulation Results

In order to examine the control effect, ADRC, FADRC, and FNNADRC are used to control the TWSBR under different road surfaces, and the simulation results are analysed and compared. The

parameters of ADRC are determined by the trial and error method, and then corrected by FNN when the system is running. The parameters of FNN are adjusted by error back-propagation. According to the stress analysis, the maximum x_1 of TWSBR is $\arctan \mu$, where μ is ground friction coefficient [7], therefore, the initial value of inclination should be less than this value. There is no restriction on the initial values of steering angle and displacement. Based on the above instructions, set the initial states $x_1 = \pi/20$, $x_3 = \pi/4$, $x_5 = 0$, desired states $x_1 = 0$, $x_3 = 0$, $x_5 = 0.5$.

4.1 Flat Road

In case of flat road surface $\alpha = 0$, ADRC, FADRC and FNNADRC are used for control simulation respectively. The upright inclination, turning angle and displacement control effects are shown in Figs. 5–7. Fig. 5 shows that the upright curves of ADRC and FADRC oscillate greatly. The error between the real dip angle and the expected value is large, while the error between the dip curve of FNNADRC and the target value is the small. There is no disturbance in the turning subsystem of TWSBR dynamic model, so the little error between the real and the expected value of turning angle in Fig. 6 is showed. Therefore, the error between the real and the expected value of the turning angle under any road condition is relatively small, and the control result is similar to Fig. 6, which will not be described later. Fig. 7 shows that the error of FNNADRC between the displacement curve and the target value is small, and it is better than that of ADRC and FADRC. In conclusion, the control effect of FNNADRC is more satisfactory than the other two methods on flat road surface.
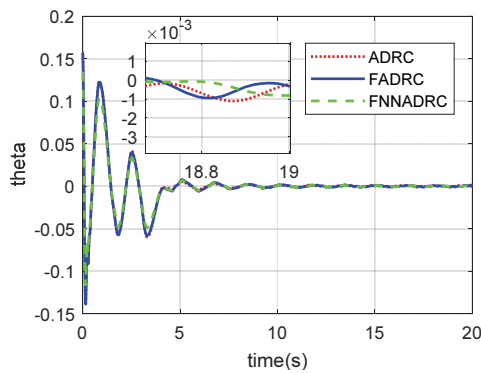
Fig. 5. Upright curve on the flat road.
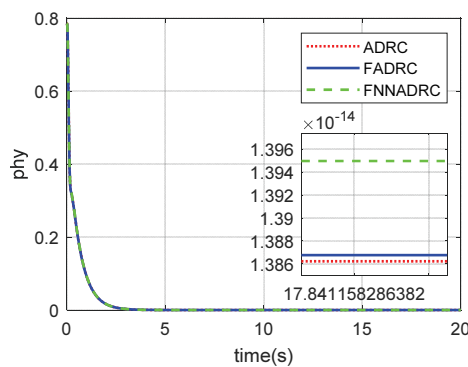
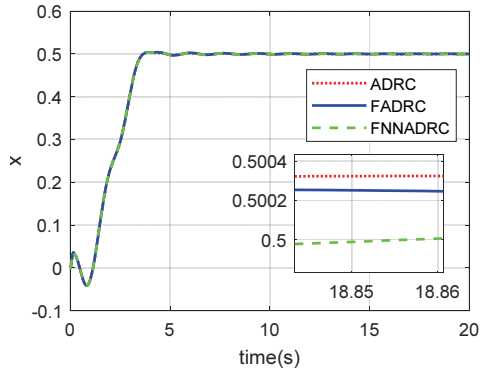**Fig. 6**. Turning curve on the flat road.

Fig. 7. Displacement curve on the flat road.

4.2 Slope Road

In case of slope road surface α = 0.174rad, ADRC, FADRC and FNNADRC are used for control simulation respectively. The control effects of upright inclination and displacement are displayed in Figs. 8 and 9. Fig. 8 exhibits that the upright curve oscillation amplitude of ADRC and FADRC is large, while the error between the inclination curve of FNNADRC and the target value is small. Fig. 8 shows that the dip and displacement curves of FNNADRC are smoother and have less errors. To sum up, FNNADRC has the best comprehensive control effect under the slope.
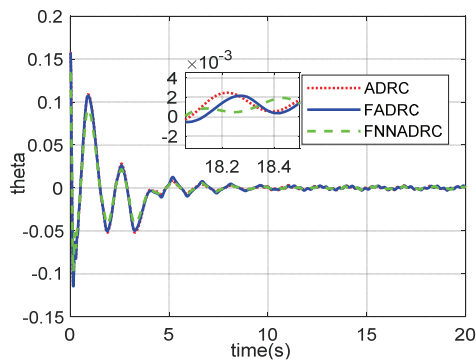

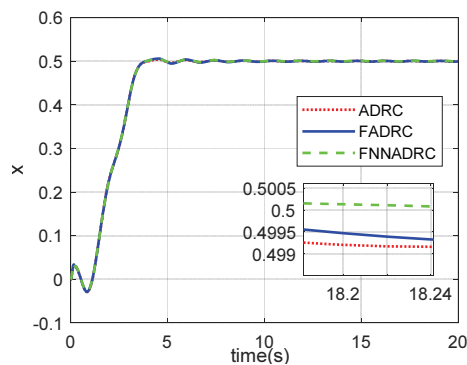**Fig. 8.** Upright curve on the slope road.

Fig. 9. Displacement curve on the slope road.

4.3 Undulating Road

Under the condition of undulating road surface $\alpha = \sin x_1$, ADRC, FADRC and FNNADRC are used for control simulation respectively. The upright inclination and displacement control effects are exhibited in Figs. 10 and 11. Fig. 10 shows that the upright curve oscillation amplitude of ADRC and FADRC is large, while the error between the inclination curve of FNNADRC and the target value is more acceptable. Fig. 11 shows that the displacement curves of ADRC and FADRC have large oscillation amplitude, while the error between the displacement curve of FNNADRC and the target value is more in line with the requirements. In summary, FNNADRC has the best comprehensive control effect under undulating road surface.
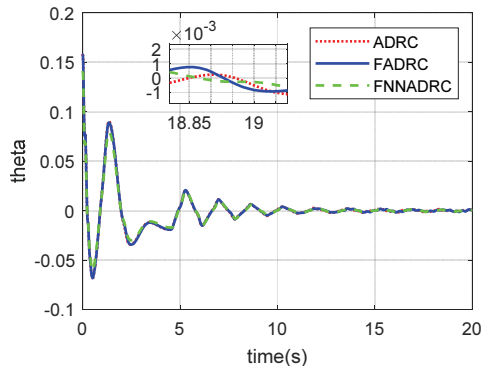
Fig. 10. Upright curve on the undulating road.
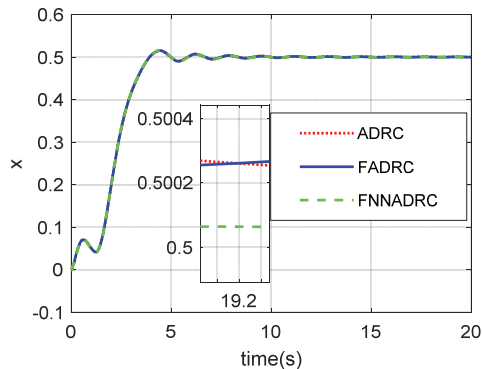
Fig. 11. Displacement curve on the undulating road.

5. Conclusion

In this research, the disturbance rejection problem of the TWSBR in complex environments is studied. According to the dynamics model of the TWSBR system on undulating pavement, the FNNADRC is designed. The nonlinear system is decoupled into three subsystems. Then, considering the characteristics of the subsystems, an ADRC is designed to ensure the stability of the subsystems. And the controller parameters are corrected by the self-learning function of the FNN. Under flat road surface, slope road

surface and undulating road surface, the control methods of ADRC, FADRC and FNNADRC are simulated and compared respectively to examine the disturbance rejection capability of FNNADRC. The results of the simulation display that FNNADRC has improved anti-interference capability compared with the other two methods.

References

[1] R. P. M. Chan, K. A. Stol, and C. R. Halkyard, "Review of modelling and control of two-wheeled robots," *Annual Reviews in Control*, vol. 37, no. 1, pp. 89-103, 2013.

[2] B. Mahler and J. Haase, "Mathematical model and control strategy of a two-wheeled self-balancing robot," in *Proceedings of the 39th Annual Conference of the IEEE Industrial Electronics Society*, Vienna, Austria, 2013, pp. 4198-4203.

[3] M. A. Imtiaz, M. Naveed, N. Bibi, S. Aziz, and S. Z. H. Naqvi, "Control system design, analysis & implementation of two wheeled self balancing robot (TWSBR)," in *Proceedings of 2018 IEEE 9th Annual Information Technology, Electronics and Mobile Communication Conference (IEMCON)*, Vancouver, Canada, 2018, pp. 431-437.

[4] C. C. Tsai, H. C. Huang, and S. C. Lin, "Adaptive neural network control of a self-balancing two-wheeled scooter," *IEEE Transactions on Industrial Electronics*, vol. 57, no. 4, pp. 1420-1428, 2010.

[5] Z. Kausar, K. Stol, and N. Patel, "The effect of terrain inclination on performance and the stability region of two-wheeled mobile robots," *International Journal of Advanced Robotic Systems*, vol. 9, no. 5, article no. 218, 2012. https://doi.org/10.5772/52894

[6] M. I. Ali and M. M. Hossen, "A two-wheeled self-balanced robot with dynamics model," in *Proceedings of 2017 4th International Conference on Advances in Electrical Engineering (ICAEE)*, Dhaka, Bangladesh, 2017, pp. 271-275.

[7] Z. Kausar, K. Stol, and N. Patel, "Performance enhancement of a statically unstable two wheeled mobile robot traversing on an uneven surface," in *Proceedings of 2010 IEEE Conference on Robotics, Automation and Mechatronics*, Singapore, 2010, pp. 156-162.

[8] J. Wu, W. Zhang, and S. Wang, "A two-wheeled self-balancing robot with the fuzzy PD control method," *Mathematical Problems in Engineering*, vol. 2012, article no. 469491, 2012. https://doi.org/10.1155/2012/469491

[9] J. Hu and G. F. Yan, "Analysis of two-wheeled self-balancing mobile robots based on ADRC," *Journal of Mechanical & Electrical Engineering*, vol. 31, no. 2, pp. 159-164, 2014.

[10] L. Jiang, H. Qiu, Z. Wu, and J. He, "Active disturbance rejection control based on adaptive differential evolution for two-wheeled self-balancing robot," in *Proceedings of 2016 Chinese Control and Decision Conference (CCDC)*, Yinchuan, China, 2016, pp. 6761-6766.

[11] A. Unluturk and O. Aydogdu, "Adaptive control of two-wheeled mobile balance robot capable to adapt different surfaces using a novel artificial neural network–based real-time switching dynamic controller," *International Journal of Advanced Robotic Systems*, vol. 14, no. 2, article no. 1729881417700893, 2017. https://doi.org/10.1177/1729881417700893

[12] D. Liang, N. Sun, Y. Wu, and Y. Fang, "Dynamic modeling and control of inverted pendulum robots moving on undulating pavements," in *Proceedings of 2017 Seventh International Conference on Information Science and Technology (ICIST)*, Da Nang, Vietnam, 2017, pp. 115-120.

[13] K. G. Tran, N. H. Nguyen, and P. D. Nguyen, "Observer-based controllers for two-wheeled inverted robots with unknown input disturbance and model uncertainty," *Journal of Control Science and Engineering*, vol. 2020, article no. 7205737, 2020. https://doi.org/10.1155/2020/7205737

[14] E. H. Karam, R. S. Habeeb, and N. Mjeed, "A new approach in design of sliding mode controller by optimization state feedback for two wheeled self balancing robot," *International Journal of Open Information Technologies*, vol. 8, no. 10, pp. 39-44, 2020.

[15] M. R. Fikri, D. W. Djamari, and S. M. Levy, "H-infinity controller design of two-wheeled mobile robot under disturbance," in *Proceedings of 2021 International Seminar on Intelligent Technology and Its Applications (ISITIA)*, Surabaya, Indonesia, 2021, pp. 147-152.

[16] Y. Wang, *Robot Intelligent Control Engineering*. Beijing, China: Science Press, 2004.

Chao Wang https://orcid.org/0000-0003-1342-9706

He received M.S. degrees in School of marine electrical engineering from Dalian Maritime University. He is a teaching assistant. His current research interests include intelligent control and Stability Analysis of Nonlinear Systems.

Xiao Jianliang https://orcid.org/0000-0001-6559-6341

He graduated from Dalian Marine University. Currently, he is an associate professor at the City Institute, Dalian University of Technology. His current research interests include network security and Artificial Intelligence.

Cheng Zhang https://orcid.org/0000-0001-8439-4892

He graduated from Dalian University of Technology. Currently, he is a professor at the City Institute, Dalian University of Technology. He has published over 20 papers in the field of digital image processing and virtual reality.